Applied Physics Letters

Direct epitaxial nanometer-thin InN of high structural quality on 4H–SiC by atomic layer deposition

Cite as: Appl. Phys. Lett. **117**, 093101 (2020); https://doi.org/10.1063/5.0014900
Submitted: 23 May 2020 . Accepted: 20 August 2020 . Published Online: 01 September 2020

Chih-Wei Hsu, Petro Deminskyi, Ivan Martinovic, Ivan G. Ivanov, Justinas Palisaitis, and Henrik Pedersen

Applied Physics Letters ARTICLE scitation.org/journal/apl

Direct epitaxial nanometer-thin InN of high structural quality on 4H–SiC by atomic layer deposition

Cite as: Appl. Phys. Lett. **117**, 093101 (2020); doi: 10.1063/5.0014900
Submitted: 23 May 2020 · Accepted: 20 August 2020 ·
Published Online: 1 September 2020

View Online Export Citation CrossMark

Chih-Wei Hsu,[a] Petro Deminskyi, Ivan Martinovic, Ivan G. Ivanov, Justinas Palisaitis, and Henrik Pedersen

AFFILIATIONS

Department of Physics, Chemistry and Biology, Linköping University, SE-58183 Linköping, Sweden

[a]Author to whom correspondence should be addressed: chih-wei.hsu@liu.se

ABSTRACT

Indium nitride (InN) is a highly promising material for high frequency electronics given its low bandgap and high electron mobility. The development of InN-based devices is hampered by the limitations in depositing very thin InN films of high quality. We demonstrate growth of high-structural-quality nanometer thin InN films on 4H–SiC by atomic layer deposition (ALD). High resolution x-ray diffraction and transmission electron microscopy show epitaxial growth and an atomically sharp interface between InN and 4H–SiC. The InN film is fully relaxed already after a few atomic layers and shows a very smooth morphology where the low surface roughness (0.14 nm) is found to reproduce sub-nanometer surface features of the substrate. Raman measurements show an asymmetric broadening caused by grains in the InN film. Our results show the potential of ALD to prepare high-quality nanometer-thin InN films for subsequent formation of heterojunctions.

Group III-nitrides are highly important semiconducting materials for electronic and optoelectronic devices. The low bandgap of InN[1] allows light-emitting-diodes (LEDs), with high In-content InGaN or InN as active layers, to operate in the near infrared regime and facilitates new photovoltaic and photocatalytic applications.[2] The high electron saturation velocity and high mobility of InN, predicted up to 12 000 $cm^2/V\,s$,[3] make InN very interesting for high-frequency devices. Modeling has predicted that the two-dimensional electron gas (2DEG) density, electron localization, and 2DEG mobility can be greatly enhanced by either inserting a single layer of InN between AlGaN and GaN in a high electron mobility structure or using an electron channel of up to 5 nm of InN, if the underlying buffer layer could prevent InN from relaxation.[4,5] High-quality nanometer thin InN layers are, therefore, of high interest for future LED and high-frequency transistor technologies.

The growth of homogeneous nanometer thin InN layers suffers from a large lattice mismatch to common templates and substrates for group III-nitride epitaxy. Furthermore, In-adatoms have high surface diffusivity and high self-cohesive force, meaning that metallic In droplets are prone to form. Deposition of InN is also hampered by the low decomposition temperature of InN. Therefore, InN deposition typically results in separated crystalline islands or films with high density of structural defects. Chemical vapor deposition,[6,7] hydride vapor phase epitaxy,[8] sputtering,[9] and molecular beam epitaxy[10,11] (MBE) have been employed for growth of InN to study the bulk properties. MBE has also been used to prepare InN monolayers embedded in a GaN matrix for short-period superlattices.[12] However, the knowledge and deposition techniques for just-a-few-nanometer InN films are still at their infant stage.

Recently, atomic layer deposition (ALD) has emerged as a promising method for the growth of AlN,[13] GaN,[14,15] and InN.[16,17] The ALD approach, characterized by the alternating introduction of the group III and the nitrogen precursors separated by inert purge gas between pulses, fully depends on surface chemical reactions, eliminating gas phase reactions between the different precursors. The hallmark of ALD is also a perfectly conformal film on topographically complex substrates, potentially opening up for more complex device structures.

Here, we present homogeneous, wurtzite InN layers epitaxially grown on on-axis 4H–SiC (0001) by ALD. 4H–SiC possesses type-I band alignment with respect to InN, which could be a promising substrate to initiate the InN heterojunctions for device applications.[18] The growth of InN is done by ALD at 320 °C and 6 mbar in a Picosun

R-200 advanced ALD system as previously described.[19] The ALD system is equipped with a commercial microwave plasma generator with an adjustable power range between 300 and 3000 W. Trimethyl indium (TMI) and (NH_3 + Ar) plasma were used to provide In and N, respectively, for complete reaction of InN. Double-side polished with a Si-face chemical-mechanical polished, on-axis 4H–SiC (0001) substrate used in this work was commercially acquired in test grade from Norstel AB. The 4H–SiC (0001) substrate was chemically cleaned using a standard RCA cleaning procedure before loading into the reactor. After stabilization at 320 °C for 60 min and prior to the growth of InN, the 4H-SiC (0001) substrate was subjected to (100 sccm Ar + 50 sccm N_2) 2800 W plasma treatment for 2 min to remove residual surface oxide. After the plasma treatment, the system was purged with 100 sccm N_2 for 10 s followed by the first TMI pulse. An ALD cycle comprises 4 s TMI pulse, 10 s N_2 purge, 12 s (50 sccm NH_3 + 100 sccm Ar) 2800 W plasma exposure, and 6 s N_2 purge. The ALD cycle was repeated in different times to obtain InN with different thicknesses as shown in Fig. 1. It should be mentioned that InN grown under this condition reveals better structural and morphological properties than others within the growth window that we reported in Ref. 19. In addition, a fill-empty step for TMI pulses was employed to facilitate the flow of TMI.[19] More information related to the growth process can be found in the supplementary material.

Figure 1 shows the XRD 2θ-ω scan of InN on 4H–SiC with different numbers of ALD cycles. The diffraction peaks at 31.3° and 35.58° can be indexed to the relaxed wurtzite InN (0002) planes and to the (0004) planes of the 4H–SiC substrate, respectively. Given that the critical thickness of InN on 4H–SiC is less than one monolayer,[12] a relaxed InN film is expected. However, 2.3 nm InN is seemingly compressively strained as the profile shifts toward a lower 2θ angle. Metallic In, which is a common inclusion in InN thin films or on the surface, seen as a peak at 33°, is not detected in our films.[11] On the other hand, no peak is observed in a grazing incidence XRD (GI-XRD) 2θ scan in the range of 20–90° using a fixed 0.5° incident angle under current geometry. By tilting the sample 90° ($\chi = 90°$), the diffraction peaks associated with $(10\bar{1}0)$ and $(11\bar{2}0)$ of InN should be revealed under their corresponding orientations. According to the hexagonal crystalline nature of InN, the occurrence of both $(10\bar{1}0)$ and $(11\bar{2}0)$ would exhibit sixfold symmetry by fixing $2\theta - \omega$ to corresponding angles of either $(10\bar{1}0)$ and $(11\bar{2}0)$ planes and performing in-plane rotation scans ($\varphi = 0 - 360°$). In addition to their respective set of sixfold symmetric peaks, a 30° offset is expected between these two sets. To prove the epitaxial relationship between InN and SiC, the angles for the occurrence of InN are expected to be identical to that of SiC. According to our experimental results (see the supplementary material, Figs. S1–S3), all the criteria described above are fulfilled. Wurtzite InN grown epitaxially on the 4H–SiC substrate is concluded based on our XRD results. The multiple satellite peaks in the vicinity of InN (0002), as seen in Fig. 1, are thickness-correlated fringes caused by the interference between InN and 4H–SiC (0001). The simulated profiles match well with our experimental results, suggesting a smooth surface and sharp interface in our case (see the supplementary material, Fig. S4).

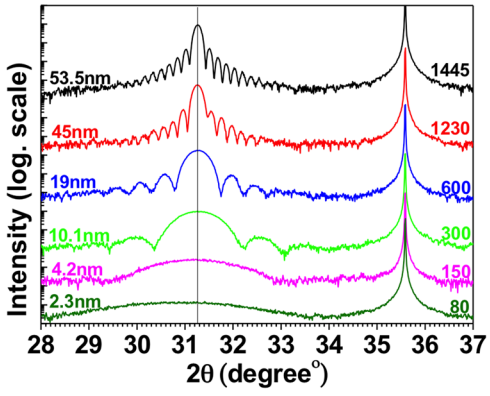

FIG. 1. X-ray diffractograms of 2θ-ω scan of InN films grown with different numbers of ALD cycles on 4H–SiC (0001). The number of ALD cycles and their corresponding film thicknesses determined by fringes are indicated, respectively, in the plot. The curves are plotted on the log scale and are shifted vertically for visual clarity.

Despite the pronounced broadening of the InN (0002) peak in 2θ-ω scan, the full-width at half-maximum (FWHM) of InN (0002) in the ω-scan does not show any significant broadening even when the InN film thickness is less than 5 nm (see the supplementary material, Fig. S5). A comparable FWHM for InN (0002) and 4H–SiC (0004) suggests that no significant amount of screw- and mixed-type threading dislocations is generated during the growth of InN. The shape of ω-scan curves of the InN follows those of their 4H–SiC substrates, indicating that the inherent "mis-orientations of SiC" are duplicated by the InN films. Our XRD ω-scan results further suggest that the degree of coherence of InN stacking is determined by the underlying 4H–SiC (0001) substrate.

The atomically sharp interface between 4H–SiC and InN is seen in the HR-STEM lattice-resolved micrograph in Fig. 2(a). The corresponding Fast Fourier transform (FFT) diffractograms [inset in Fig. 2(a)] prove that the AB-type (2H) stacking of InN and the ABAC-type (4H) stacking of the 4H–SiC substrate are well-aligned along the [0001] and $[01\bar{1}0]$ direction, confirming the hetero-epitaxy. According to our FFT diffractogram, the lattice mismatch between InN and SiC substrates is 14.7% along $[11\bar{2}0]$ (a-direction), in good agreement with that derived from reported values for relaxed InN[20] and 4H–SiC substrates. Owing to the large lattice mismatch, the strain relaxation is expected to take place at a very early stage of InN growth. Misfit dislocations are commonly seen at the interface in our study. The Burgers circuit analysis around individual misfits indicated the Burgers vector of $b = a\langle 01\bar{1}0\rangle$ association with edge dislocation as shown in Fig. 2(b). This type of misfit can be observed periodically at the interface, which could be visualized by the filtered inverse FFT image [IFFT, Fig. 2(c)]. These edge-type misfit dislocations are known to be the most common and efficient defect for strain relaxation at interfaces with a large lattice mismatch as has been observed in InN/AlN[21] and other material systems.[22,23] The only other structural defects observed are some regions where certain atomic columns do not show well-distinguished projections as indicated by the blue arrows in Fig. 2(d). We believe that these are in-plane irregularities related to point defects caused by the coalescence between separate grains of monolayers in order to minimize the energy, a consequence of the extremely low growth rate (0.37 Å per ALD cycle), and so the imperfections such as vacancies and impurities are introduced at boundaries without any distinguishable Burger vectors. It should be mentioned that the dark contrast propagating along the growth direction in the STEM image is not associated with threading dislocations. Instead, they reflect the

In-deficient nature due to high-angle annular dark-field imaging. Indium vacancies and impurities of light elements are speculated to be the point defects. This argument is supported by our Raman results, which will be discussed later.

Figure 3(a) shows a representative top view SEM image of a 20 nm InN film deposited on (0001) 4H–SiC. The contrast of the image is weak, indicating that our InN film is smooth and is free from the common surface non-homogeneities such as large crystal grains and In-rich droplets.[6,11] It should be mentioned that non-optimal ALD growth conditions will lead to a rougher surface and In-rich clusters as observed in the literature.[24] A smooth surface is further shown by the topographical atomic force micrograph of the InN surface [Fig. 3(b)]. The root-mean square (RMS) roughness of the 20 nm thick InN film is 0.16 nm. For comparison, the root-mean square roughness of the bare 4H–SiC substrate is 0.13 nm. We find that the RMS roughness of InN is independent of the thickness of InN in this study. The surface stepping feature of 4H–SiC caused by the CMP process finished at the substrate supplier [inset in Fig. 3(b)] is duplicated by the InN film, showing the conformity of the InN growth at the nanometer scale.

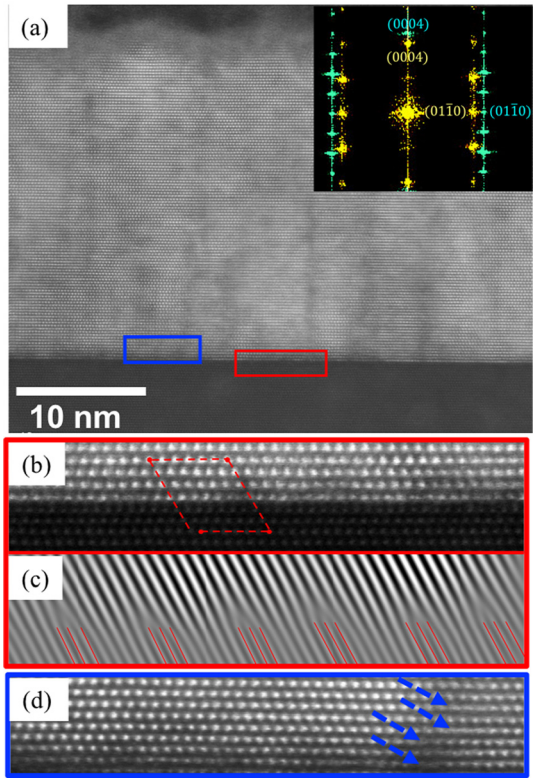

FIG. 2. (a) HR-STEM image from the InN film grown on 4H–SiC; the corresponding FFT is shown in the inset. The golden pattern in FFT is associated with InN while the cyan pattern with 4H–SiC. (b) Magnified image from the interface region as depicted by the red box in (a). The Burger circuit analysis is depicted by the dashed lines. (c) The corresponding filtered IFFT image of (b). Misfit takes place regularly as indicated by the red line. (d) Lattice-resolved image of first 9 layers of InN. The blue arrows point out where the atomic-column projections are not well-resolved.

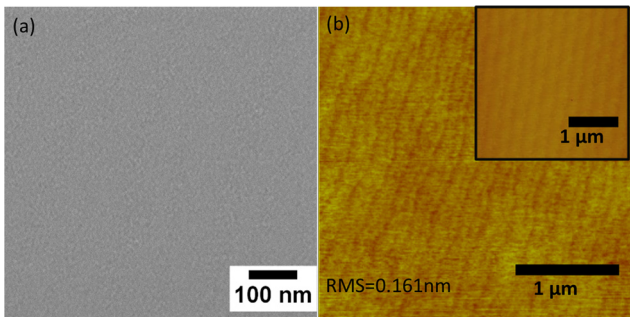

FIG. 3. (a) A representative top-view SEM image of a 20 nm InN film grown on the 4H–SiC substrate. (b) An AFM micrograph of a 20 nm InN film grown on the 4H–SiC substrate, inset: an AFM micrograph of a 4H–SiC substrate prior to the growth of InN.

Raman spectroscopy was conducted to study the vibrational properties and the strain status of the films. The spectra are shown in Fig. 4, where the spectrum of a bare 4H–SiC substrate is also shown for reference (the bottom curve). Two of the Raman modes allowed in the backscattering geometry, E_2(high) and A_1(LO), are observed in all samples, but instead of sharp peaks, we observe significantly broadened bands peaking approximately at 585 cm^{-1} and 489 cm^{-1}, close to the positions of these modes in a relaxed, single-crystalline wurtzite InN grown along the *c*-direction.[25] The A_1(TO) Raman mode is forbidden in the backscattering geometry, but appears in our spectra as a band positioned around 450 cm^{-1}. Both the broadening of the Raman modes and the appearance of the forbidden A_1(TO) can be understood by the grained structure of the films. According to our TEM analysis, the grains are on the nanometer scale defined by the thickness and the "in-plane irregularities." The existence of grains aligned along the c-axis but coalesced laterally with respect to each other implies defects associated with the positioning boundaries between the individual grains. Hence, inhomogeneous strain distribution within the film is expected, which leads to inhomogeneous broadening of the Raman peaks. In addition, the selection rules could be

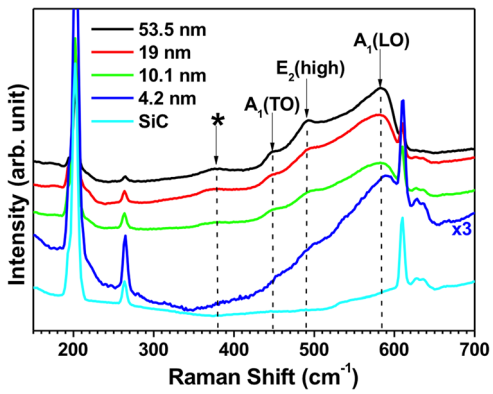

FIG. 4. Raman spectra of InN films with different thicknesses. The spectrum of the bare 4H–SiC substrate is also included for comparison. The Raman modes also observable in bulk InN are denoted in the graph, and their corresponding peak positions are guided by dashed lines. A 532 nm laser is used, and the measurement configuration is $Z(X,.)\bar{Z}$. The results are shifted vertically for visual clarity.

relaxed by the deformation potential originating from the small displacement of atoms from their equilibrium positions. Such a phenomenon has been observed in nano-crystals[26] or GaN films with anisotropic strain.[27] Finally, a band centered around 380 cm^{-1} is also observed. In a previous study, the appearance of this band has been associated with localized gap mode due to In vacancies.[28] This suggestion is somewhat in line with the In-deficient nature observed in our TEM image.

A clear shift of approximately 5 cm^{-1} toward the higher wavenumber for A_1(LO) is observed in the 4.2 nm InN film. Such a shift can be due to the presence of compressive strain within the film and/or the coupled longitudinal optical phonon-plasmon mode (LPP+).[29] It should be mentioned that all Raman signals we observed are much broader than the typical linewidth from bulk counterparts.[25] The pronounced asymmetric broadening can be due to the combined effects of disorder-activated scattering caused by various grain sizes in the ultra-thin InN layer,[30] surface optical modes of InN,[31] and Fano interference caused by discrete phonon modes and background continuum electron transitions in the system.[32,33] Despite the fact that our XRD results support the presence of compressive strain, the contribution of LPP+ cannot be ruled out due to the surface accumulation effect especially for InN nanostructures.[26] Further studies are under way to unveil the thickness-dependent optical and electrical properties of InN.

In summary, the growth of nanometer-thin epitaxial InN films with very high structural quality on (0001) 4H–SiC by ALD is reported. InN is seen to relax in the first layer via the formation of misfit dislocations on 4H–SiC followed by a nearly homoepitaxial stacking of InN. An atomically sharp and smooth InN/4H–SiC interface is seen by both XRD and TEM. A high structural quality is demonstrated even for a 2.3 nm InN film. The ALD process renders excellent uniformity of the macroscopic surface morphology. According to our TEM and Raman spectroscopy, inhomogeneous stress conditions caused by point defects at grain boundaries are suggested to be responsible for the inhomogeneous Raman broadening and for the relaxation of the selection rules leading to the observation of the A1(TO) mode. Our results highlight the advantage of ALD to prepare homogeneous, epitaxial InN nano-layers on foreign substrates.

See the supplementary material for the detailed information related to the growth process and XRD results that support the heteroepitaxy between InN and SiC.

This work was financially supported by the Swedish Foundation for Strategic Research through the project "Time-resolved low temperature CVD for III-nitrides" (No. SSF-RMA 15-0018) and by the Knut and Alice Wallenberg foundation through the project "Bridging the THz gap" (No. KAW 2013.0049). I.G.I. acknowledges support from the VR (Project No. VR 2016-05362). P.D. acknowledges the Carl Trygger Foundation for a postdoctoral scholarship at Linköping University. The authors acknowledge the Knut and Alice Wallenberg Foundation for support of the Linköping electron microscopy laboratory.

DATA AVAILABILITY

The data that support the findings of this study are available from the corresponding author upon reasonable request.

REFERENCES

[1]J. Wu, W. Walukiewicz, K. M. Yu, J. W. Ager, I. I. I. E. E. Haller, H. Lu, W. J. Schaff, Y. Saito, and Y. Nanishi, Appl. Phys. Lett. **80**, 3967 (2002).
[2]E. Trybus, G. Namkoong, W. Henderson, S. Burnham, W. A. D. little, M. Cheung, and A. Cartwright, J. Cryst. Growth **288**, 218218 (2006).
[3]S. Wang, H. Liu, Q. Chen, and H. Zhang, J. Mater. Sci. **27**, 11353–11357 (2016).
[4]M. S. Miao and C. G. Van de Walle, Appl. Phys. Express **8**, 024302 (2015).
[5]J. Kuzmik and A. Georgakilas, IEEE Trans. Electron Devices **58**, 720 (2011).
[6]A. Jain, S. Raghavan, and J. M. Redwing, J. Cryst. Growth **269**, 128–133 (2004).
[7]C. Yang, X. Wang, H. Xiao, X. Zhang, G. Hu, J. Ran, C. Wang, J. Li, and Z. Wang, Appl. Surf. Sci. **255**, 3149–3152 (2008).
[8]R. Togashi, Q. T. Thieu, H. Murakami, Y. Kumagai, Y. Ishitanic, B. Monemar, and A. Koukitu, J. Cryst. Growth **422**, 15–19 (2015).
[9]M. Amirhoseiny, Z. Hassan, S. S. Ng, and G. Alahyarizadeh, Surf. Rev. Lett. **20**, 1350008 (2013).
[10]T. Ive, O. Brandt, M. Ramsteiner, M. Giehler, H. Kostial, and K. H. Ploog, Appl. Phys. Lett. **84**, 1671 (2004).
[11]P. Jantawongrit, S. Sanorpim, H. Yaguchi, M. Orihara, and P. Limsuwan, J. Semicond. **36**, 083002 (2015).
[12]A. Yoshikawa, S. B. Che, W. Yamaguchi, H. Saito, X. Q. Wang, Y. Ishitani, and E. S. Hwang, Appl. Phys. Lett. **90**, 073101 (2007).
[13]N. Nepal, S. B. Qadri, J. K. Hite, N. A. Mahadik, M. A. Mastro, and C. R. Eddy, Jr., Appl. Phys. Lett. **103**, 082110 (2013).
[14]C. Ozgit, I. Donmez, M. Alevli, N. Biyikli, C. Ozgit, I. Donmez, M. Alevli, and N. Biyikli, J. Vac. Sci. Technol., A **30**, 01A124 (2012).
[15]S. Liu, G. Zhao, Y. He, H. Wei, Y. Li, P. Qiu, Y. Song, Y. An, X. Wang, X. Wang, J. Cheng, M. Peng, and X. Zheng, ACS Appl. Mater. Interfaces **11**, 35382–35388 (2019).
[16]N. Nepal, N. A. Mahadik, L. O. Niyakiti, S. B. Qadri, M. J. Mehl, J. K. Hite, and C. R. Eddy, Jr., Cryst. Growth Des. **13**, 1485 (2013).
[17]A. Haider, S. Kizir, and N. Biyikli, AIP Adv. **6**, 045203 (2016).
[18]B. L. Zhang, G. S. Sun, Y. Guo, P. F. Zhang, R. Q. Zhang, H. B. Fan, X. L. Liu, S. Y. Yang, Q. S. Zhu, and Z. G. Wang, Appl. Phys. Lett. **93**, 242107 (2008).
[19]P. Deminskyi, P. Rouf, I. Ivanov, and H. Pedersen, J. Vac. Sci. Technol., A **37**, 020926 (2019).
[20]M. A. Moram and M. E. Vickers, Rep. Prog. Phys. **72**, 036502 (2009).
[21]V. Lebedev, V. Cimalla, J. Pezoldt, M. Himmerlich, S. Krischok, J. A. Schaefer, O. Ambacher, F. M. Morales, J. G. Lozano, and D. González, J. Appl. Phys. **100**, 094902 (2006).
[22]J. Li, G. Miao, Y. Zeng, Z. Zhang, D. Li, H. Song, H. Jiang, Y. Chen, X. Suna, and Z. Li, CrystEngComm **19**, 88 (2017).
[23]A. Rocher and E. Snoeck, Mater. Sci. Eng., B **67**, 62–69 (1999).
[24]Y. An, Y. He, H. Wei, S. Liu, M. Li, Y. Song, P. Qiu, A. Rehman, X. Zheng, and M. Peng, Results Phys. **12**, 804–809 (2019).
[25]V. Y. Davydov, V. V. Emtsev, I. N. Goncharuk, A. N. Smirnov, V. D. Petrikov, M. B. Smirnov, and T. Inushima, Appl. Phys. Lett. **75**, 3297 (1999).
[26]K. K. Madapu, S. R. Polaki, and S. Dhara, Phys. Chem. Chem. Phys. **18**, 18584–18589 (2016).
[27]V. Darakchieva, T. Paskova, M. Schubert, H. Arwin, P. P. Paskov, B. Monemar, D. Hommel, M. Heuken, J. Off, F. Scholz, B. A. Haskell, P. T. Fini, J. S. Speck, and S. Nakamura, Phys. Rev. B **75**, 195217 (2007).
[28]J. B. Wang, Z. F. Li, P. P. Chen, W. Lu, and T. Yao, Acta Mater. **55**, 183 (2007).
[29]Y. M. Chang, C. T. Chuang, C. T. Chia, K. T. Tsen, H. Lu, and W. J. Schaff, Appl. Phys. Lett. **85**, 5224 (2004).
[30]J. Chen, W. Z. Shen, J. B. Wang, H. Ogawa, and Q. X. Guo, J. Cryst. Growth **262**, 435–441 (2004).
[31]S. Sahoo, M. S. Hu, C. W. Hsu, C. T. Wu, K. H. Chen, L. C. Chen, A. K. Arora, and S. Dhara, Appl. Phys. Lett. **93**, 233116 (2008).
[32]A. E. Miroshnichenko, S. Flach, and Y. S. Kivshar, Rev. Mod. Phys. **82**, 2257–2298 (2010).
[33]T. Inushima, M. Higashiwaki, and T. Matsui, Phys. Rev. B **68**, 235204 (2003).